

# Fano-type resonances induced by a boson mode in Andreev conductance

J. Barański and T. Domański

*Institute of Physics, M. Curie-Skłodowska University, 20-031 Lublin, Poland*

(Dated: September 4, 2014)

We study spectroscopic signatures of a monochromatic boson mode interacting with a T-shape double quantum dot coupled between the metallic and superconducting leads. Focusing on a weak interdot coupling we find that the proximity effect together with bosonic mode are responsible for series of the Fano-type resonances appearing simultaneously at negative and positive energies. We investigate these interferometric features and discuss their influence on the subgap Andreev conductance taking into account the correlation effects driven by the Coulomb repulsion.

Keywords: Fano interference, Andreev scattering, polaronic features

PACS numbers: 73.63.Kv;73.23.Hk;74.45.+c;74.50.+r

## I. INTRODUCTION

Fano-type interference arises when a discrete level is combined with a broad spectrum, giving rise to the asymmetric spectroscopic shapes [1]. Such interferometric structures attract presently substantial interests in the studies of electron propagation through disordered systems [2], STM data for the Kondo-type impurities [3], spectra of the heavy fermion compounds [4], charge/spin transport through nanoscopic systems [5] etc. In this work we analyze the Fano-type lineshapes appearing in the subgap spectrum and tunneling conductance of a double quantum-dot coupled between a normal (N) and superconducting (S) electrode, as shown in figure 1. In particular we examine how the bosonic bath (assumed as a monochromatic mode) combines with the proximity induced pairing and the strong electron interactions.

Under nonequilibrium conditions charge can be transmitted between the external (N and S) electrodes either via the usual single particle tunneling (if applied voltage  $V$  is sufficiently large to break the electron pairs,  $|eV| \geq \Delta$ ) or by activating the anomalous Andreev channel. In the latter case electrons from the normal electrode are converted into Cooper pairs in the superconducting lead, simultaneously reflecting the holes back to metallic electrode. Differential conductance of such Andreev current is sensitive to both, the induced on-dot pairing and the electron correlations [6–9]. This issue has been studied theoretically for the single quantum dot [10–15] (see also other references cited therein) and the double quantum dot heterojunctions [16–22].

Since nanoscopic objects (quantum dots, nanowires or molecules) are never entirely separated from their environment (e.g. photon [23] or vibron [24] quanta) therefore transport properties can reveal additional features originating from the constructive/destructive interference. In this work we study the system (Fig. 1), where a direct electron transport occurs via the central quantum dot (QD<sub>1</sub>) and a weak leakage to the side-coupled quantum dot (QD<sub>2</sub>) contributes the interference effects. Similar mechanism has been investigated for the case with both

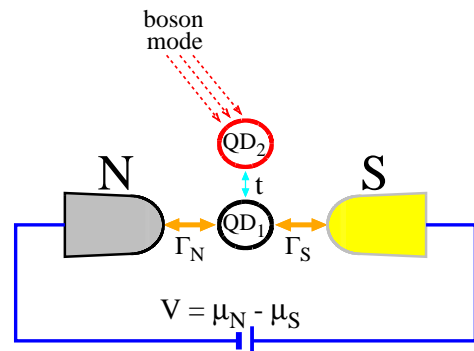


FIG. 1: (color online) Schematic view of the T-shape double quantum dot coupled between the metallic (N) and superconducting (S) electrodes, where the side-attached dot (QD<sub>2</sub>) is affected by a monochromatic boson mode (e.g. vibrons).

normal electrodes [25, 26] predicting the Fano-type resonances in the differential conductance, as has been indeed confirmed experimentally [27].

When the quantum dots are hybridized with a superconducting reservoir one expects the interference patterns simultaneously in the particle and hole sectors, because of the induced on-dot pairing [28, 29]. We have already analyzed such interferometric Fano resonances considering dephasing due to the external fermionic bath [30]. In the present work we extend such study taking into account the external bosonic mode.

In section II we introduce the model and specify the characteristic energy scales. Next, we discuss formal aspects related the approximations. In section IV we present signatures of the boson mode for the uncorrected quantum dots. Finally, in section V, we consider the correlation effects (including the Kondo regime). Appendix provides a simple phenomenological explanation of the Fano-type interferometric lineshapes of the heterojunctions consisting of two weakly coupled quantum dots.

## II. MICROSCOPIC MODEL

The heterojunction shown in figure 1 can be described by the following microscopic Hamiltonian

$$\hat{H} = \hat{H}_N + \hat{H}_S + \hat{H}_{DQD} + \hat{H}_T \quad (1)$$

where  $\hat{H}_N$  ( $\hat{H}_S$ ) refers to the normal (superconducting) charge reservoir,  $\hat{H}_{DQD}$  describes the quantum dots together with a boson bath and the last term  $\hat{H}_T$  corresponds to hybridization of the central QD<sub>1</sub> to external leads. We treat the conducting lead as a Fermi gas  $\hat{H}_N = \sum_{\mathbf{k},\sigma} \xi_{\mathbf{k}N} \hat{c}_{\mathbf{k}\sigma N}^\dagger \hat{c}_{\mathbf{k}\sigma N}$  and describe the isotropic superconductor by the BCS Hamiltonian  $\hat{H}_S = \sum_{\mathbf{k},\sigma} \xi_{\mathbf{k}S} \hat{c}_{\mathbf{k}\sigma S}^\dagger \hat{c}_{\mathbf{k}\sigma S} - \Delta \sum_{\mathbf{k}} (\hat{c}_{\mathbf{k}\uparrow S}^\dagger \hat{c}_{-\mathbf{k}\downarrow S}^\dagger + \hat{c}_{-\mathbf{k}\downarrow S} \hat{c}_{\mathbf{k}\uparrow S})$ , where  $\hat{c}_{\mathbf{k}\sigma\beta}^{(\dagger)}$  denote the annihilation (creation) operators of mobile electrons with spin  $\sigma = \uparrow$  or  $\downarrow$ . The energies  $\xi_{\mathbf{k}\beta} = \varepsilon_{\mathbf{k}\beta} - \mu_\beta$  are measured with respect to the chemical potentials  $\mu_\beta$ , where  $\mu_N - \mu_S = eV$ .

We assume that external bosonic bath directly affects only the side-attached quantum dot (QD<sub>2</sub>). Hamiltonian of the quantum dots and such bosonic mode is given by

$$\begin{aligned} \hat{H}_{DQD} = & \sum_{\sigma,i} \varepsilon_i \hat{n}_{i\sigma} + \sum_i U_i \hat{n}_{i\uparrow} \hat{n}_{i\downarrow} + \omega_0 \hat{a}^\dagger \hat{a} \\ & + t \sum_{\sigma} \left( \hat{d}_{1\sigma}^\dagger \hat{d}_{2\sigma} + \text{H.c.} \right) + \lambda \sum_{\sigma} \hat{n}_{2\sigma} (\hat{a}^\dagger + \hat{a}). \end{aligned} \quad (2)$$

$\hat{d}_i^{(\dagger)}$  are the annihilation (creation) operators of QD <sub>$i=1,2$</sub>  electrons,  $\hat{a}^{(\dagger)}$  refer to the bosonic mode and  $\hat{n}_{i\sigma} = \hat{d}_{i\sigma}^\dagger \hat{d}_{i\sigma}$ . As usually  $\varepsilon_i$  denote the energy levels,  $\lambda$  is a coupling of the boson mode with QD<sub>2</sub>, and  $\omega_0$  is the bosonic energy. In what follows we shall analyze the Fano-type interference originating from a weak coupling between both quantum dots (see the Appendix for details)

$$\hat{H}_T = \sum_{\beta=N,S} \sum_{\mathbf{k},\sigma} \left( V_{\mathbf{k}\beta} \hat{d}_{1\sigma}^\dagger \hat{c}_{\mathbf{k}\sigma\beta} + \text{H.c.} \right). \quad (3)$$

The model (1) can be generalized to more complex situations, for instance when both quantum dots are coupled to the external leads [14, 20] and to the boson mode. For clarity we focus on the case illustrated in figure 1, because it represents the simplest realization of the Fano-type lineshapes originating from the bosonic mode.

## III. OUTLINE OF THE FORMALISM

To study the electronic spectrum and the transport properties of the system (1) we introduce the matrix Green's function  $\mathbf{G}_i(\tau_1, \tau_2) = -i\hat{T}_\tau \langle \hat{\Psi}_i(\tau_1) \hat{\Psi}_i^\dagger(\tau_2) \rangle$  in the Nambu representation  $\hat{\Psi}_i^\dagger \equiv (\hat{d}_{i\uparrow}^\dagger, \hat{d}_{i\downarrow}^\dagger)$ ,  $\hat{\Psi}_i \equiv (\hat{\Psi}_i^\dagger)^\dagger$ . In equilibrium conditions ( $\mu_N = \mu_S$ ) the Green's function depends only on time difference  $\tau_1 - \tau_2$  and its Fourier transform can be expressed as

$$\mathbf{G}_i^{-1}(\omega) = \mathbf{g}_i^{-1}(\omega) - \Sigma_i^0(\omega) - \Sigma_i^{corr}(\omega), \quad (4)$$

where the bare Green's functions  $\mathbf{g}_i(\omega)$  are given by

$$\mathbf{g}_i(\omega) = \begin{pmatrix} \omega - \varepsilon_i & 0 \\ 0 & \omega + \varepsilon_i \end{pmatrix}^{-1}. \quad (5)$$

The first part of the selfenergy  $\Sigma_i^0(\omega)$  comes from the hybridizations and the second term  $\Sigma_i^{corr}(\omega)$  is due to the correlation effects.

### A. Uncorrelated quantum dots

Let us start with the selfenergies  $\Sigma_i^0(\omega)$  of the uncorrelated quantum dots, that are solvable exactly. We can express them as

$$\Sigma_1^0(\omega) = |t|^2 \mathbf{G}_2(\omega) + \sum_{\mathbf{k}} \sum_{\beta=N,S} |V_{\mathbf{k}\beta}|^2 \mathbf{g}_\beta(\mathbf{k}, \omega), \quad (6)$$

$$\Sigma_2^0(\omega) = |t|^2 \mathbf{G}_1(\omega), \quad (7)$$

where  $\mathbf{g}_\beta(\mathbf{k}, \omega)$  denote the Green's functions of the leads. For the normal lead  $\mathbf{g}_N(\mathbf{k}, \omega)$  has a diagonal structure

$$\mathbf{g}_N(\mathbf{k}, \omega) = \begin{pmatrix} \frac{1}{\omega - \xi_{\mathbf{k}N}} & 0 \\ 0 & \frac{1}{\omega + \xi_{\mathbf{k}N}} \end{pmatrix} \quad (8)$$

and for the superconductor  $\mathbf{g}_S(\mathbf{k}, \omega)$  takes the BCS form

$$\mathbf{g}_S(\mathbf{k}, \omega) = \begin{pmatrix} \frac{u_{\mathbf{k}}^2}{\omega - E_{\mathbf{k}}} + \frac{v_{\mathbf{k}}^2}{\omega + E_{\mathbf{k}}} & \frac{-u_{\mathbf{k}}v_{\mathbf{k}}}{\omega - E_{\mathbf{k}}} + \frac{u_{\mathbf{k}}v_{\mathbf{k}}}{\omega + E_{\mathbf{k}}} \\ \frac{-u_{\mathbf{k}}v_{\mathbf{k}}}{\omega - E_{\mathbf{k}}} + \frac{u_{\mathbf{k}}v_{\mathbf{k}}}{\omega + E_{\mathbf{k}}} & \frac{u_{\mathbf{k}}^2}{\omega + E_{\mathbf{k}}} + \frac{v_{\mathbf{k}}^2}{\omega - E_{\mathbf{k}}} \end{pmatrix} \quad (9)$$

with the gaped quasiparticle energies  $E_{\mathbf{k}} = \sqrt{\xi_{\mathbf{k}S}^2 + \Delta^2}$  and the coefficients  $u_{\mathbf{k}}^2, v_{\mathbf{k}}^2 = \frac{1}{2} \left[ 1 \pm \frac{\xi_{\mathbf{k}S}}{E_{\mathbf{k}}} \right]$ ,  $u_{\mathbf{k}}v_{\mathbf{k}} = \frac{\Delta}{2E_{\mathbf{k}}}$ .

In the wide band limit one can introduce the constant hybridization functions  $\Gamma_\beta = 2\pi \sum_{\mathbf{k}} |V_{\mathbf{k}\beta}|^2 \delta(\omega - \xi_{\mathbf{k}\beta})$ . Formally we then obtain

$$\sum_{\mathbf{k}} |V_{\mathbf{k}N}|^2 \mathbf{g}_\beta(\mathbf{k}, \omega) = -i \frac{\Gamma_N}{2} \begin{pmatrix} 1 & 0 \\ 0 & 1 \end{pmatrix} \quad (10)$$

$$\sum_{\mathbf{k}} |V_{\mathbf{k}S}|^2 \mathbf{g}_S(\mathbf{k}, \omega) = -i \frac{\Gamma_S}{2} \gamma(\omega) \begin{pmatrix} 1 & \frac{\Delta}{\omega} \\ \frac{\Delta}{\omega} & 1 \end{pmatrix} \quad (11)$$

with the auxiliary function [10]

$$\gamma(\omega) = \begin{cases} \frac{|\omega|}{\sqrt{\omega^2 - \Delta^2}} & \text{for } |\omega| > \Delta, \\ \frac{\omega}{i\sqrt{\Delta^2 - \omega^2}} & \text{for } |\omega| < \Delta. \end{cases} \quad (12)$$

Deep in a subgap regime (i.e. for energies  $|\omega| \ll \Delta$ ) the expression (11) simplifies to a purely off-diagonal structure with the following static terms  $-\Gamma_S/2$ . One can hence interpret  $|\Gamma_S/2| \equiv \Delta_{d1}$  as the pairing gap induced in the central quantum dot [10, 12].

## B. Influence of a boson mode

To take into account the boson mode we first determine the selfenergy  $\Sigma_2^{corr}(\omega)$  of the side-attached quantum dot, neglecting the inter-dot coupling  $t$ . For convenience we introduce the molecular Hamiltonian

$$\hat{H}_{mol} = \varepsilon_2 \hat{n}_{2\sigma} + U_2 \hat{n}_{2\uparrow} \hat{n}_{2\downarrow} + \omega_0 \hat{a}^\dagger \hat{a} + \lambda \sum_{\sigma} \hat{n}_{2\sigma} (\hat{a}^\dagger + \hat{a}) \quad (13)$$

and use the unitary transformation  $e^{\hat{S}} \hat{H}_{mol} e^{-\hat{S}} = \hat{\tilde{H}}_{mol}$  to eliminate the electron-boson coupling. Adopting the Lang-Firsov generating operator [31]

$$\hat{S} = \frac{\lambda}{\omega_0} \sum_{\sigma} \hat{d}_{2\sigma}^\dagger \hat{d}_{2\sigma} (\hat{a}^\dagger - \hat{a}) \quad (14)$$

one obtains [32]

$$\hat{\tilde{H}}_{mol} = \sum_{\sigma} \tilde{\varepsilon}_2 \hat{d}_{2\sigma}^\dagger \hat{d}_{2\sigma} + \tilde{\omega}_0 \hat{a}^\dagger \hat{a} + \tilde{U}_2 \hat{n}_{2\uparrow} \hat{n}_{2\downarrow} \quad (15)$$

with the renormalized energy  $\tilde{\varepsilon}_2 = \varepsilon_2 - \lambda^2/\omega_0$  and effective potential  $\tilde{U}_2 = U_2 - 2\lambda^2/\omega_0$ . Additionally, the operators

$$\hat{d}_{\sigma}^{(\dagger)} = \hat{d}_{\sigma}^{(\dagger)} \hat{X}^{(\dagger)}, \quad \hat{a}^{(\dagger)} = \hat{a}^{(\dagger)} - \frac{\lambda}{\omega_0} \sum_{\sigma} \hat{d}_{\sigma}^\dagger \hat{d}_{\sigma}, \quad (16)$$

are *dressed* with the polaronic cloud

$$\hat{X} = e^{-(\lambda/\omega_0)(\hat{a}^\dagger - \hat{a})}. \quad (17)$$

In absence of the interdot coupling we can exactly determine the Green's function  $\mathbf{G}_2(\omega)$  using the identity

$$\begin{aligned} \langle \hat{T}_{\tau} \hat{d}_{\sigma}(\tau_1) \hat{d}_{\sigma}^\dagger(\tau_2) \rangle_{\hat{H}_{mol}} &= \langle \hat{T}_{\tau} \hat{d}_{\sigma}(\tau_1) \hat{d}(\tau_2)^\dagger \rangle_{\hat{\tilde{H}}_{mol}} \\ &= \langle \hat{T}_{\tau} \hat{d}_{\sigma}(\tau_1) \hat{d}_{\sigma}^\dagger(\tau_2) \rangle_{fer.} \langle \hat{T}_{\tau} \hat{X}(\tau_1) \hat{X}^\dagger(\tau_2) \rangle_{bos.} \end{aligned} \quad (18)$$

with  $\hat{T}_{\tau}$  being the time ordering operator. The first part of equation (18) expresses invariance of the trace  $\langle \dots \rangle_{\hat{H}_{mol}} = \langle \dots \rangle_{\hat{\tilde{H}}_{mol}}$  under the unitary transformation. The second line of (18) comes from the fact that statistical averaging with respect to the transformed Hamiltonian (15) is exactly equal to a product of the average with respect to the bosonic and the fermionic degrees of freedom. In particular, the polaronic propagator acquires the following standard form [32]

$$\begin{aligned} \langle \hat{T}_{\tau} \hat{X}(\tau_1) \hat{X}^\dagger(\tau_2) \rangle &= \exp \{ -(\lambda/\omega_0)^2 \\ &\times [(1 - e^{-i\omega_0(\tau_1 - \tau_2)})(1 + N_p) + (1 - e^{i\omega_0(\tau_1 - \tau_2)})N_p] \} \end{aligned} \quad (19)$$

with the Bose-Einstein distribution  $N_p = [e^{\beta\omega_0} - 1]^{-1}$ . This result (19) can be used to compute the Fourier

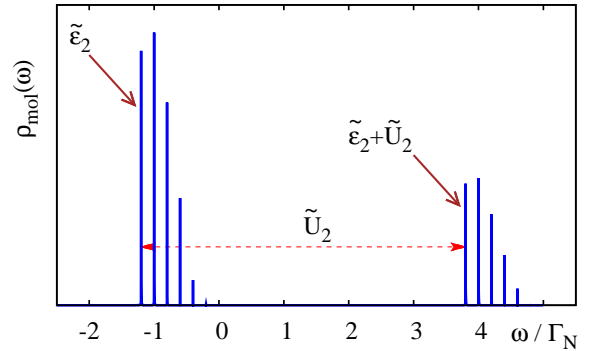


FIG. 2: (color online) The molecular spectral function obtained at zero temperature using the following set of parameters  $\varepsilon_2 = -1\Gamma_N$ ,  $U_2 = 5\Gamma_N$ ,  $\omega_0 = 0.2\Gamma_N$ ,  $g = 1$ ,  $\varepsilon_1 = 0$ .

transform of the molecular Green's function  $\mathbf{g}_{mol}(\omega) \equiv \lim_{t \rightarrow 0} \mathbf{G}_2(\omega)$ . Such propagator has a diagonal structure with the following terms [33]

$$\begin{aligned} \mathbf{g}_{mol,11}(\omega) &= e^{-(\lambda\sqrt{1+2N_p}/\omega_0)^2} \quad (20) \\ &\times \sum_l e^{l\beta\omega_0/2} I_l \left[ 2\left(\frac{\lambda}{\omega_0}\right)^2 \sqrt{N_p(1+N_p)} \right] \\ &\times \left( \frac{1 - \langle \hat{n}_{2\downarrow} \rangle}{\omega - \tilde{\varepsilon}_2 - l\omega_0} + \frac{\langle \hat{n}_{2\downarrow} \rangle}{\omega - \tilde{\varepsilon}_2 - \tilde{U}_2 - l\omega_0} \right) \end{aligned}$$

and  $\mathbf{g}_{mol,22}(\omega) = -[\mathbf{g}_{mol,11}(-\omega)]^*$ , where  $I_l$  denote the modified Bessel functions. At zero temperature the Green's (20) simplifies to

$$\begin{aligned} \lim_{T \rightarrow 0} \mathbf{g}_{mol,11}(\omega) &= \quad (21) \\ \sum_l e^{-g} \frac{g^l}{l!} \left( \frac{1 - \langle \hat{n}_{2\downarrow} \rangle}{\omega - \tilde{\varepsilon}_2 - l\omega_0} + \frac{\langle \hat{n}_{2\downarrow} \rangle}{\omega - \tilde{\varepsilon}_2 - \tilde{U}_2 - l\omega_0} \right) \end{aligned}$$

with the adiabaticity parameter  $g = (\lambda/\omega_0)^2$ .

Effectively the molecular spectral function  $\rho_{mol}(\omega) = -\pi^{-1} \text{Im} \mathbf{g}_{mol,11}(\omega + i0^+)$  shows two groups of the polaronic peaks (see figure 2). The lower polaronic branch starts at  $\tilde{\varepsilon}_2$  and the upper branch one is separated from it by  $\tilde{U}_2$  (because the Coulomb potential  $U_2$  is partly suppressed by the bipolaronic shift  $2\lambda^2/\omega_0$ ) [32, 33]. For the particular value  $g = 1$  we observe about five peaks, but in the antiadiabatic regime ( $g \gg 1$ ) a number of boson peaks considerably increases.

In the succeeding sections we are treating the correlation effects (driven by the bosonic mode and the Coulomb repulsion  $U_2$ ) within the following approximation

$$\Sigma_2^{corr}(\omega) \simeq \mathbf{g}_2^{-1}(\omega) - \mathbf{g}_{mol}^{-1}(\omega) \quad (22)$$

which shall be reliable for the weak interdot coupling  $t$ .

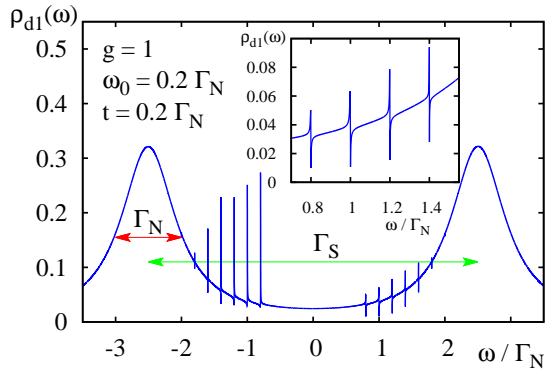


FIG. 3: (color online) The interferometric Fano-type lineshapes of the spectral function  $\rho_{d1}(\omega)$  of QD<sub>1</sub> obtained at  $T = 0$  for the uncorrelated quantum dots ( $U_i = 0$ ) using  $\varepsilon_1 = 0$ ,  $\varepsilon_2 = 1\Gamma_N$ ,  $t = 0.2\Gamma_N$ ,  $\Gamma_S = 5\Gamma_N$  and  $\Delta = 10\Gamma_N$ .

### C. Subgap transport

In a subgap regime  $|eV| < \Delta$  electrons are transmitted between the external electrodes practically only via the Andreev channel. Such anomalous current  $I_A(V)$  can be expressed by the Landauer-type formula [34–36]

$$I_A(V) = \frac{2e}{h} \int d\omega T_A(\omega) [f(\omega - eV) - f(\omega + eV)], \quad (23)$$

where  $f(\omega) = [e^{\omega/k_B T} + 1]^{-1}$  is the Fermi-Dirac distribution. Andreev transmittance  $T_A(\omega)$  depends on the off-diagonal part of the Green's function  $\mathbf{G}_1(\omega)$  via [34]

$$T_A(\omega) = \Gamma_N^2 |G_{1,12}(\omega)|^2. \quad (24)$$

Roughly speaking, (24) is a quantitative measure of the induced on-dot pairing and its optimal values coincide with the quasiparticle energies of the in-gap states). This transmittance  $T_A(\omega)$  depends also on the effects related to the quantum interference [19, 21, 22, 30].

Experimental measurements usually probe the differential conductance  $G_A(V) = \frac{\partial I_A(V)}{\partial V}$ . We now discuss the spectrum and the tunneling conductance  $G_A(V)$  of the double quantum dot system: i) neglecting both Coulomb interactions  $U_i$  (section IV) and ii) treating the electron-electron repulsion by suitable approximations (section V). Let us notice that  $T_A(-\omega) = T_A(\omega)$  implies the symmetric Andreev conductance  $G_A(-V) = G_A(V)$ . This property comes from the fact that particle and hole states equally participate in the Andreev scattering.

## IV. UNCORRELATED QUANTUM DOTS

In absence of both Coulomb interactions  $U_i$  we can determine the matrix Green's functions  $\mathbf{G}_i(\omega)$  using the Dyson equation (4) with the selfenergies (6, 7). We treat

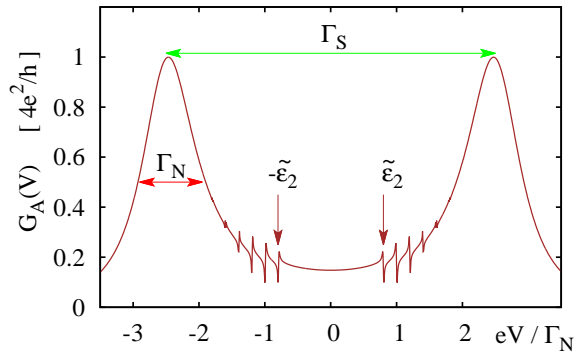


FIG. 4: (color online) The subgap Andreev conductance  $G_A(V)$  obtained for the same parameters as in figure 3.

the influence of a boson mode through the local solution (22), assuming  $U_2 = 0$ . For small interdot coupling  $t \ll \Gamma_\beta$  the induced pairing affects mainly the low energy states of central dot (QD<sub>1</sub>), therefore we focus on the case  $\varepsilon_1 = 0$ ,  $\varepsilon_2 \neq \varepsilon_1$ . Figure 3 shows the equilibrium spectrum  $\rho_{d1}(\omega)$  obtained at zero temperature for  $g = \lambda/\omega_0 = 1$  assuming the small boson energy  $\omega_0 < \Delta$ . Such case is interesting because the interferometric patterns appear in the subgap Andreev spectroscopy. Let us emphasize that the boson mode considered here is not related with the origin of superconductivity of the external lead. Such low energy boson mode could either represent the vibrational mode or the electromagnetic *ac* field. Such subgap vibration modes have been indeed reported experimentally for the carbon nanotubes suspended between external electrodes [37, 38]. For the single quantum dot heterojunctions this situation has been studied theoretically in Refs [39–42].

We notice two Lorentzian peaks at the quasiparticle energies  $\pm\Gamma_S/2$  and two series of the Fano resonances. Such resonances appear at energies  $\pm(\tilde{\varepsilon}_2 + l\omega_0)$  because of the particle - hole mixed excitations [28]. Number of these interferometric features is sensitive to the adiabaticity parameter  $g$ . In the adiabatic regime ( $g \leq 1$ ) there appear only a few features, whereas in the antiadiabatic limit their number considerably increases. The Fano-type lineshapes appear also in the Andreev conductance (see Fig. 4). In comparison with the spectral function  $\rho_{d1}(\omega)$  the resonances are symmetrized for the reasons mentioned in the preceding section. Measurements of the subgap Andreev conductance would thus be able to detect such boson induced interferometric features.

The in-gap quasiparticle peaks (often referred as *the bound Andreev states*) depend on the energy level  $\varepsilon_1$ . In the case of single quantum dot (i.e. for vanishing  $t$ ) the spectral function  $\rho_{d1}(\omega)$  consists of two Lorentzians at  $\pm E_1$  (where  $E_1 = \sqrt{\varepsilon_1^2 + (\Gamma_S/2)^2}$ ) broadened by  $\Gamma_N$ . Their spectral weights are given by the BCS factors  $\frac{1}{2}(1 \pm \varepsilon_1/E_1)$ . This property has also influence on the interferometric features. Figure 5 shows the spectrum  $\rho_{d1}(\omega)$  for several values of  $\varepsilon_1$ . When the energy level  $\varepsilon_1$

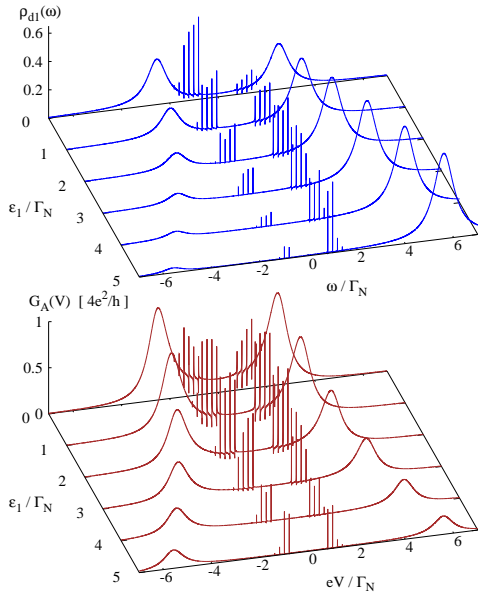


FIG. 5: (color online) Dependence of the spectral function  $\rho_{d1}(\omega)$  and the Andreev conductance  $G_A(V)$  on  $\varepsilon_1$  (tunable by the gate voltage) for the same parameters as in Fig. 4.

is more distant from the Fermi level we observe a gradual redistribution of the quasiparticle spectral weights accompanied with suppression of the Fano resonances, especially at  $-(\tilde{\varepsilon}_2 + l\omega_0)$ . The Andreev conductance  $G_A(V)$  is even function of the voltage  $V$  therefore such particle-hole redistribution is not well pronounced, however suppression of the boson induced Fano lineshapes is noticeable.

## V. CORRELATION EFFECTS

In this last section we discuss additional effects caused by the Coulomb repulsion  $U_i$ . Since electron transport occurs via the central quantum dot we expect  $U_1$  to play the most significant role. For completeness we separately analyze the qualitative effects originating from both Coulomb potentials  $U_i$ .

### A. $U_1 = 0, U_2 \neq 0$

In order to study the influence of  $U_2$  we simply use the approximate selfenergy (22), which is reliable in the case of weak interdot coupling. For stronger couplings  $t \geq \Gamma_\beta$  one should rather adopt eigen-basis of the double quantum dot and consider higher order correlation effects, like e.g. an indirect exchange interaction (between QD<sub>2</sub> and the metallic reservoir) which could induce the exotic Kondo effect [43]. This interesting aspect, however, goes beyond a scope of the present study.

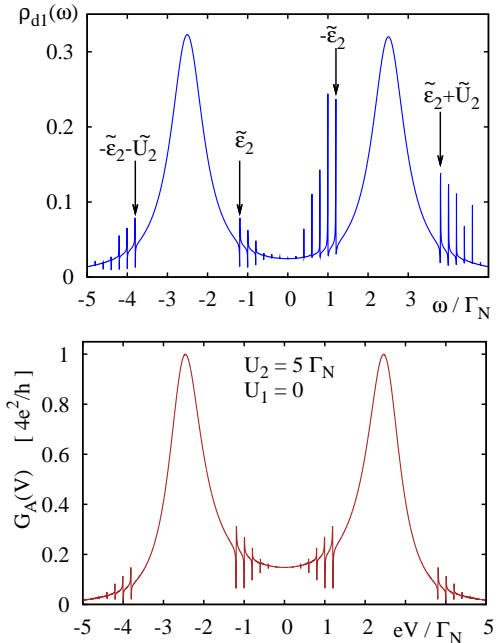


FIG. 6: (color online) Spectral function  $\rho_{d1}(\omega)$  of the central quantum dot (top panel) and the differential Andreev conductance (bottom panel) obtained at zero temperature for  $\varepsilon_1 = 0$ ,  $\varepsilon_2 = -1\Gamma_N$ ,  $t = 0.2\Gamma_N$ ,  $g = 1$ ,  $\omega_0 = 0.2\Gamma_N$ ,  $\Delta = 10\Gamma_N$ , and  $U_2 = 5\Gamma_N$ .

The upper panel of figure 6 illustrates the QD<sub>1</sub> spectrum  $\rho_{d1}(\omega)$  obtained at zero temperature for  $U_2 = 5\Gamma_N$ ,  $U_1 = 0$ . As far as the spectrum of QD<sub>2</sub> is concerned it still consists of two series of the bosonic peaks appearing around  $\tilde{\varepsilon}_2$  and near the Coulomb satellite  $\tilde{\varepsilon}_2 + \tilde{U}_2$ , similar to what is shown figure 2 except a finite broadening of the peaks  $\sim t^2/D$ .

The Fano-type resonances appearing in  $\rho_{d1}(\omega)$  result from a combined effect of the interference (caused by the side attached quantum dot) and the proximity induced on-dot pairing. We can notice effectively four groups of such structures appearing near  $\pm\tilde{\varepsilon}_2$  and  $\pm(\tilde{\varepsilon}_2 + \tilde{U}_2)$  due to the particle-hole mixing. These Fano structures show up also in the Andreev conductance  $G_A(\omega)$ , though in a symmetrized way (bottom panel in Fig. 6).

### B. $U_1 \neq 0, U_2 = 0$

The potential  $U_1$  has a qualitatively different influence on the transport properties than  $U_2$ . The central quantum dot is coupled between N and S leads therefore it is affected by the on-dot pairing (promoted by  $\Gamma_S$ ) and by the effective exchange interaction (due to finite  $\Gamma_N$  and  $U_1$ ) leading to the Kondo effect. These phenomena are antagonistic. Their competition has been so far addressed by various groups using different many-body techniques (see e.g. [12] for a survey).

Here we analyze spectroscopic features of the system

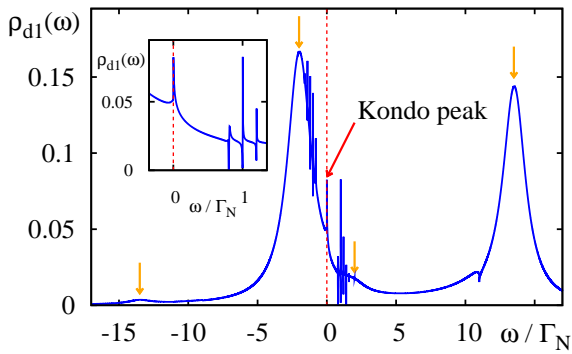


FIG. 7: (color online) Spectral function  $\rho_{d1}(\omega)$  of QD<sub>1</sub> obtained in the Kondo regime for  $k_B T = 10^{-3}\Gamma_N$ ,  $\varepsilon_1 = -2\Gamma_N$ ,  $U_2 = 15\Gamma_N$ ,  $\Gamma_S = 4\Gamma_N$ ,  $t = 0.2\Gamma_N$ ,  $\omega_0 = 0.2\Gamma_N$ ,  $g = 1$ ,  $\Delta \gg \Gamma_N$ . Vertical arrows indicate quasiparticle energies of the Andreev states (at  $\pm E_1$  and their Coulomb satellites). We can notice the Kondo peak at  $\omega = 0$  coexisting with a number of the Fano-type resonances induced by the boson mode.

(Fig. 1) following our studies [44–47] based on the equation of motion technique (EOM) [48]. Such approximation proved to give satisfactory results for the single quantum dot heterojunctions [7, 8]. We thus assume the correlation selfenergy  $\Sigma_{1,11}^{corr}(\omega)$  in a diagonal form with

$$\begin{aligned} \Sigma_{1,11}^{corr}(\omega) &= U_1 [n_{1\downarrow} - \Sigma_1(\omega)] \\ &+ \frac{U_1 [n_{1\downarrow} - \Sigma_1(\omega)] [\Sigma_3(\omega) + U_1(1 - n_{1\downarrow})]}{\omega - \varepsilon_1 - \Sigma_0(\omega) - [\Sigma_3(\omega) + U_1(1 - n_{1\downarrow})]} \end{aligned} \quad (25)$$

and  $\Sigma_{1,22}^{corr}(\omega) = -[\Sigma_{1,11}^{corr}(-\omega)]^*$ . The other symbols appearing in (25) have the following meanings [48]  $\Sigma_0(\omega) = \sum_{\mathbf{k}} |V_{\mathbf{k}N}|^2 / (\omega - \xi_{\mathbf{k}N}) \simeq -i\Gamma_N/2$  and

$$\begin{aligned} \Sigma_\nu(\omega) &= \sum_{\mathbf{k}} |V_{\mathbf{k}N}|^2 \left[ \frac{1}{\omega - \xi_{\mathbf{k}N}} + \frac{1}{\omega - U_1 - 2\varepsilon_1 + \xi_{\mathbf{k}N}} \right] \\ &\times \begin{cases} f(\xi_{\mathbf{k}N}) & \text{for } \nu = 1, \\ 1 & \text{for } \nu = 3. \end{cases} \end{aligned} \quad (26)$$

Eqn. (25) qualitatively captures both the Coulomb blockade and the Kondo effect, when  $\varepsilon_1 < 0 < \varepsilon_1 + U_1$  and  $T \leq T_K \sim 0.29\sqrt{U_1\Gamma_N}/2 \exp\left[\frac{\pi\varepsilon_1(\varepsilon_1 + U_1)}{\Gamma_N U_1}\right]$ . Under such conditions there appears a narrow Abrikosov-Suhl peak at  $\omega = 0$  whose broadening is scaled by  $k_B T_K$ . The EOM treatment is however not reliable in reproducing the low energy shape of this peak, that could be obtained from the numerical renormalization group calculations [10, 29] or other many-body methods [49–55].

Let us briefly point out the characteristic properties of the Kondo regime. Spectral function of the central quantum dot (shown in Fig. 7) consists of four Lorentzians at energies of the Andreev bound states indicated by the arrows. Such quasiparticle subgap states are formed at

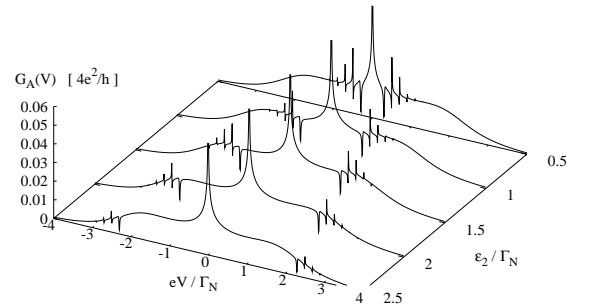


FIG. 8: (color online) Differential conductance of the Andreev current obtained in the Kondo regime for the same set of parameters as in figure 7 and for varying  $\varepsilon_2$ .

$\pm\sqrt{\varepsilon_1^2 + (\Gamma_S/2)^2}$  and  $\pm\sqrt{(\varepsilon_1 + U_1)^2 + (\Gamma_S/2)^2}$ . We have chosen  $\varepsilon_1$  slightly below the Fermi level therefore the quasiparticle spectral weights are not symmetric. Apart of the Lorentzians we notice the narrow Kondo peak at the Fermi level. It is considerably reduced in comparison to the normal case  $\Delta=0$  because of the competition between pairing and spin ordering [44]. Finally, we additionally recognize the Fano-type interference patterns at  $\pm(\tilde{\varepsilon}_2 + l\omega_0)$ .

These features show up also in the subgap Andreev conductance. Figure 8 shows maxima of  $G_A(V)$  at voltages corresponding to the quasiparticle energies of the Andreev bound states. Moreover, we notice the additional zero-bias enhancement due to the Kondo effect which has been indeed observed experimentally [8]. On top of such behavior there appear the Fano-type resonances. They can have detrimental effect on the zero-bias Kondo feature when these interferometric features appear near the Fermi energy. We would like to emphasize also that this zero-bias anomaly is visible only when  $\Gamma_N \sim \Gamma_S$  [45].

## VI. SUMMARY AND OUTLOOK

We have investigated the spectrum and Andreev conductance of the T-shape double quantum dot coupled between one metallic and another superconducting electrode. Focusing on the low energy (subgap) regime we have studied influence of a bosonic mode coupled to the side-attached quantum dot, converting its spectrum to multilevel structure. Electrons tunneling through the central quantum dot are resonantly scattered (in a weak interdot coupling regime) by such multilevel ‘molecule’, giving rise to the Fano-type interference patterns.

The effective spectrum of central quantum dot and the differential conductance of N-DQD-S junction reveal groups of the equidistant bosonic resonances formed nearby  $\pm(\tilde{\varepsilon}_2 + l\omega_0)$  and  $\pm(\tilde{\varepsilon}_2 + \tilde{U}_2 + l\omega_0)$ . Correlation effects due to the Coulomb potential  $U_1$  do also significantly affect the spectroscopic properties. Spin of

the central quantum dot is screened (at low temperatures) by itinerant electrons of the metallic lead provided that proximity induced pairing (promoting the BCS-type configurations) does not completely suppress it [29]. Quantum interference eventually obscures it whenever the Fano-type resonances appear close enough to the Kondo peak.

It would be worthwhile to extend our study to the case of stronger interdot coupling. Both quantum dots (as a whole) might then be characterized by new molecular eigen-states where the boson mode could manifest itself in a qualitatively different way, no longer resembling the Fano-type resonances. Under such circumstances the Coulomb potential  $U_2$  could play as much important role as  $U_1$  via the indirect exchange interaction allowing for exotic realizations of the Kondo effect [43].

### Acknowledgment

We kindly thank S. Andergassen, B.R. Bulka, and K.I. Wysokiński for instructive discussions. This project has been supported by the National Center of Science through the grant NN202 263138.

### Appendix A: Fano resonances of DQD junctions

Let us simply explain the origin of interferometric Fano structures showing up in the transport properties of the DQD systems. Such characteristic lineshapes [56] usually emerge whenever some localized (resonant) electron waves interfere with a continuum (or with a broad electron spectrum). To provide explicit arguments let us consider the useful example [57], where the 'di-

rect' transmission channel  $t_d = \sqrt{G_d}e^{i\phi_d}$  ( $G_d$  denotes its conductance and  $\phi_d$  stands for an arbitrary phase) is superposed with the transmission amplitude  $t_r(\omega) = \sqrt{G_r} \frac{(\Gamma_L + \Gamma_R)/2}{\omega - \varepsilon_r + i(\Gamma_L + \Gamma_R)/2}$  of the 'resonant' level  $\varepsilon_r$ . The corresponding conductance can be expressed by the popular formula [48]  $G_r = \frac{2e^2}{h} \frac{4\Gamma_L\Gamma_R}{(\Gamma_L + \Gamma_R)^2}$ . Combining these two channels one obtains the characteristic function

$$G(\omega) = |t_d + t_r(\omega)|^2 = G_d \frac{|\tilde{\omega} + q|^2}{\tilde{\omega}^2 + 1} \quad (\text{A1})$$

with the auxiliary argument  $\tilde{\omega} = 2(\omega - \varepsilon_r)/(\Gamma_L + \Gamma_R)$  and the asymmetry factor  $q = i + e^{-i\phi_d} \sqrt{\frac{G_r}{G_d}}$ .

We can apply similar reasoning to the T-shape double quantum dot system shown in Fig. 1. Neglecting the phonon bath let us assume for simplicity that both electrodes are metallic conductors. For the weak interdot coupling  $t$  the side-attached dot QD<sub>2</sub> plays a role of the 'resonant' channel whose transmission amplitude is  $t_r(\omega) = \sqrt{G_r} \frac{t/2}{\omega - \varepsilon_2 + it/2}$ , where  $G_r = \frac{2e^2}{h}$ . On the other hand QD<sub>1</sub> contributes a broad background with the following effective transmission  $t_d(\omega) = \sqrt{\frac{2e^2}{h} \frac{4\Gamma_N\Gamma_S}{(\Gamma_N + \Gamma_S)^2} \frac{(\Gamma_N + \Gamma_S)/2}{\omega - \varepsilon_1 + i(\Gamma_N + \Gamma_S)/2}}$ . For energies  $\omega \sim \varepsilon_2$  the latter amplitude is nearly constant  $t_d(\omega) \simeq \sqrt{G_d}e^{i\phi_d}$  with  $\sqrt{G_d} = \sqrt{\frac{2e^2}{h} \frac{4\Gamma_N\Gamma_S}{(\Gamma_N + \Gamma_S)^2} \left| \frac{1}{2(\varepsilon_1 - \varepsilon_2) + i(\Gamma_N + \Gamma_S)} \right|}$ . Thus the resulting conductance  $G(\omega) = |t_d + t_r(\omega)|^2$  is indeed characterized by the Fano-type function (A1). Microscopic arguments explaining the origin of the Fano-type interference patterns in the strongly correlated quantum dots have been discussed at length e.g. by Maruyama [25] and by Žitko [26].

- 
- [1] Miroshnichenko A E, Flach S and Kivshar Y S 2010 *Rev. Mod. Phys.* **82** 2257
  - [2] Poddubny A N, Rybin M V, Limonov M F and Kivshar Y S 2012 *Nature Commun.* **3** 914
  - [3] Ujsaghy O, Kroha J, Szunyogh L and Zawadowski A 2000 *Phys. Rev. Lett.* **85** 2557
  - [4] Wölffe P, Dubi Y and Balatsky A V 2010 *Phys. Rev. Lett.* **105** 246401
  - [5] Katsumoto S 2007 *J. Phys.: Condens. Matter* **19** 233201
  - [6] Pillet J -D, Quay C H L, Morfin P, Bena C, Levy Yeyati A and Joyez P 2010 *Nat. Phys.* **6** 965
  - [7] Deacon R S, Tanaka Y, Oiwa A, Sakano R, Yoshida K, Shibata K, Hirakawa K and Tarucha S 2010 *Phys. Rev. Lett.* **104** 076805
  - [8] Deacon R S, Tanaka Y, Oiwa A, Sakano R, Yoshida K, Shibata K, Hirakawa K and Tarucha S 2010 *Phys. Rev. B* **81** 121308(R)
  - [9] Lee E J H, Jiang X, Aguado R, Katsaros G, Lieber Ch M and De Franceschi S 2012 *Phys. Rev. Lett.* **109** 186802
  - [10] Yamada Y, Tanaka Y and Kawakami N 2011 *Phys. Rev. B* **84** 075484;
  - [11] Oguri A, Tanaka Y and Bauer J 2013 *Phys. Rev. B* **87** 075432
  - [12] Martín-Rodero A and Levy Yeyati A 2011 *Adv. Phys.* **60** 899;
  - [13] Koerting V, Andersen B M, Flensberg K and Paaske J 2010 *Phys. Rev. B* **82** 245108
  - [14] Droste S, Andergassen S and Splettstoesser J 2012 *J. Phys.: Condens. Matter* **24** 415301
  - [15] Moghaddam A G, Governale M and König J 2012 *Phys. Rev. B* **85** 094518
  - [16] Tanaka Y, Kawakami N and Oguri A 2008 *Phys. Rev. B* **78** 035444
  - [17] Kormanyos A, Grace I and Lambert C J 2009 *Phys. Rev. B* **79** 075119
  - [18] Tanaka Y, Kawakami N and Oguri A 2010 *Phys. Rev. B* **81** 075404
  - [19] Barański J and Domański T 2011 *Phys. Rev. B* **84** 195424
  - [20] Bai L, Zhang R and Duan C -L 2012 *Nanoscale Research Letters* **7** 670
  - [21] Michałek G and Bulka B R 2012 *Acta Phys. Polon. A* **122** 981

- [22] Calle A M, Pacheco M and Orellana P A 2013 *Phys. Lett. A* **377** 1474
- [23] Platero G and Aguado R 2004 *Phys. Rep.* **395** 1
- [24] Galperin M, Ratner M A and Nitzan A 2007 *J. Phys.: Condens. Matter* **19** 103201
- [25] Maruyama I, Shibata N and Ueda K 2004 *J. Phys. Soc. Jpn.* **73** 3239
- [26] Žitko R 2010 *Phys. Rev. B* **81** 115316
- [27] Sasaki S, Tamura H, Akazaki T and Fujisawa T 2009 *Phys. Rev. Lett.* **103** 266806
- [28] Balatsky A V, Vekhter I and Zhu J -X 2006 *Rev. Mod. Phys.* **78** 373
- [29] Bauer J, Oguri A and Hewson A C 2008 *J. Phys.: Condens. Matter* **19** 486211
- [30] Barański J and Domański T 2012 *Phys. Rev. B* **85** 205451
- [31] Lang I G and Firsov Y A 1963 *Sov. Phys. JETP* **16** 1301
- [32] Mahan G D 2000 *Many-Particle Physics* (New York: Kluwer Academic/Plenum Publishers) pp. 218–228
- [33] Fransson J 2010 *Non-Equilibrium Nano-Physics: A Many-Body Approach* (Dordrecht: Springer) pp. 107–115
- [34] Krawiec M and Wysokiński K I 2004 *Supercond. Sci. Technol.* **17** 103
- [35] Sun Q -F, Guo H and Lin T -H 2001 *Phys. Rev. Lett.* **87** 176601
- [36] Sun Q -F, Wang J and Lin T -H 1999 *Phys. Rev. B* **59** 3831
- [37] Leturcq R, Stampfer C, Inderbitzin K, Durrer L, Hierold C, Mariani E, Schultz M G, von Oppen F and Ensslin K 2009 *Nature Phys.* **5** 327
- [38] Beebe J M, Kim B S, Gadzuk J W, Frisbie C D and Kushmerick J G 2006 *Phys. Rev. Lett.* **97** 026801
- [39] Zhang S N, Pei W, Fang T F and Sun Q F 2012 *Phys. Rev. B* **86** 104513
- [40] Wu B H, Cao J C and Timm C 2012 *Phys. Rev. B* **86** 035406
- [41] Dong B, Ding G H and Lei X L 2013 *Phys. Rev. B* **88** 075414
- [42] Wang Q, Xie H, Jiao H and Nie Y -H 2013 *EPL* **101** 47008
- [43] Tanaka Y, Kawakami N and Oguri A 2012 *Phys. Rev. B* **85** 155314
- [44] Barański J and Domański T 2013 *J. Phys.: Condens. Matter* **25** 435305
- [45] Domański T and Donabidowicz A 2008 *Phys. Rev. B* **78** 073105
- [46] Domański T, Donabidowicz A and Wysokiński K I 2008 *Phys. Rev. B* **78** 144515
- [47] Domański T, Donabidowicz A and Wysokiński K I 2007 *Phys. Rev. B* **76** 104514
- [48] Haug H J W and Jauho A -P 2008 *Quantum Kinetics in Transport and Optics of Semiconductors* (Berlin: Springer) pp. 205–212
- [49] Meng T, Florens S and Simon P 2009 *Phys. Rev. B* **79** 224521
- [50] Karrasch C, Andergassen S and Meden V 2011 *Phys. Rev. B* **84** 134512
- [51] Cuevas J C, Levy Yeyati A and Martín-Rodero A 2001 *Phys. Rev. B* **63** 094515
- [52] Kajueter H and Kotliar G 1996 *Phys. Rev. Lett.* **77** 131
- [53] Aligia A A 2006 *Phys. Rev. B* **74** 155125
- [54] Martín-Rodero A, Levy Yeyati A, Flores F and Monreal R C 2008 *Phys. Rev. B* **78** 235112
- [55] Górski G and Mizia J 2013 *Physica B* **427** 42
- [56] Göres J, Goldhaber-Gordon D, Heemeyer S, Kastner M A, Shtrikman H, Mahalu D and Meirav U 2000 *Phys. Rev. B* **62** 2188
- [57] Clerk A A, Waintal X and Brouwer P W 2001 *Phys. Rev. Lett.* **86** 4636